Available online at www.sciencedirect.com

SciVerse ScienceDirect

Ceramics International 39 (2013) 5205–5212

CERAMICS INTERNATIONAL

www.elsevier.com/locate/ceramint

Enhancement of antimicrobial and long-term biostability of the zinc-incorporated hydroxyapatite coated 316L stainless steel implant for biomedical application

S. Sutha, G. Karunakaran, V. Rajendran*

Centre for Nano Science and Technology, K.S. Rangasamy College of Technology, Tiruchengode 637 215, Tamil Nadu, India

Received 28 September 2012; received in revised form 4 December 2012; accepted 6 December 2012
Available online 23 December 2012

Abstract

Antimicrobial hydroxyapatite (HAp) nanoparticles with different concentrations (0, 3, and 6 mol%) of zinc were prepared by the ultrasonication process. The prepared nanoparticles and chitosan (CTS) composite were coated on 316L stainless steel implant by spin coating technique. The powder samples were characterised by particle size analyser, X-ray fluorescence, and X-ray diffraction studies. The morphology of the coating was investigated by scanning electron microscopy. The diameter of the particle size decreased with increase in the concentration of zinc in HAp structure. The structure of the coated implant was found to be uniform without any cracks and pores. Antimicrobial activity of the composites against *Bacillus subtilis*, *Staphylococcus aureus*, *Klebsiella pneumonia*, *Salmonella typhi* and *Pseudomonas aeruginosa* was analysed. The results showed that the increase in the concentration of zinc enhances the antimicrobial properties of 316L stainless steel implant. The stability of the implant in physiological environment was characterised by electrochemical impedance spectroscopy and polarisation analysis. The higher concentration of the ZnHAp/CTS composite shows higher corrosion resistance than that of the HAp/CTS-coated implant. This study shows that the coating provides corrosion resistance to the stainless steel substrate in simulated body fluid (SBF). The *in vitro* bioactivity study of the coated samples immersed in SBF solution confirms the formation of bone-like apatite layer on the surface of the implant. Thus, highly biocompatible ZnHAp/CTS-coated materials could be very useful in the long-term stability of the biomedical applications.

Keywords: B. Nanocomposites; C. Corrosion; D. Apatite; E. Biomedical applications

1. Introduction

316L stainless steel (SS) is used for restoration of anatomical structure because of its high mechanical strength, good biocompatibility and cost effective. It is widely used in the orthopaedic surgeries such as joint replacement and fracture fixation [1]. The corrosion rate of metallic implant in the human body must be negligible. Over the past two decades, the ion release and corrosion properties of metallic implant materials under physiological conditions have been extensively studied under physiological conditions [2]. The release of iron, nickel and chromium from the implant leads to unwanted reaction around the implanted area, which may cause permanent implant failure. Thus, the corrosion-resistant coating and surface modification of the implant are required [3,4]. Coating of bioactive materials using hydroxyapatite (HAp) in the metallic implant has many advantages, including improved corrosion resistance of implant surface and enhanced biointeraction with the surrounding tissues [5]. HAp is one of the naturally available biocompatible and bioactive materials that show the ability to interact with surrounding bone [6]. Low tensile strength, low mechanical properties and high dissolution rate of HAp limit its role in biomedical applications [7]. HAp contains trace amount of cations (Mn, Mg, Zn and Sr) and anions (SiO_4, H_3PO_4, and CO_3), which influence its physical properties [8]. The apatite structure has great flexibility

*Corresponding author. Tel.: +91 4288 274741x4; fax: +91 4288 274880(direct), 274860.
E-mail address: veerajendran@gmail.com (V. Rajendran).

0272-8842/$ - see front matter © 2012 Elsevier Ltd and Techna Group S.r.l. All rights reserved.
http://dx.doi.org/10.1016/j.ceramint.2012.12.019

in accepting substitution. The introduction of small quantities of ions to HAp structure improves the quality of the clinical applications [9].

Majority of the infections after orthopaedic implantation occur mainly due to the microorganisms present in the implanted materials, leading to permanent implant failure [10]. Coating of several antimicrobial ions such as copper, zinc and silver minimises bacterial load on the implant surface. The small amount of zinc is essential for metabolic processes and DNA replication, whereas its increased concentration is potentially toxic to the living organisms [11]. Zinc substitution on HAp has important implications because natural bone and teeth enamel are composed of trace amount of zinc in HAp structure [12]. The incorporation of small quantities of zinc in HAp lattice promotes bone formation around the implant and enhances mechanical strength [13]. Owing to extremely low solubility of HAp, the release of Zn ion is slow in the ZnHAp and this enhances the bone formation (osteoblast activity) around the implant [14].

To develop a homogeneous coating with high mechanical properties, we prepared an organic–inorganic composite by dispersing ceramic nanoparticles in polymer matrix [15,16]. Chitosan (CTS) is one of the highly biocompatible natural polymers that provide temporary mechanical strength to the cell in-growth [17]. Thus, its addition improves osteoblast mineralisation. Owing to this unique property, CTS has attracted great attention in the field of orthopaedic surgery. The coating of HAp ceramics with CTS at low temperature imparts chemical stability, biocompatibility and antimicrobial properties without degrading the mechanical properties of the SS substrate [18].

The aim of this study was to prepare HAp and ZnHAp nanoparticles to enhance antimicrobial properties by the ultrasonication method. The developed HAp and ZnHAp nanoparticles were mixed with CTS and coated on the 316L SS substrate by spin coating technique. Elemental composition, particle size and the functional group of the ZnHAp were determined. The corrosion stability of the HAp and ZnHAp/CTS composites coated on the SS plate in prepared simulated body fluid (SBF) was examined. The antimicrobial activity of the ZnHAp/CTS composites against bacterial strains was also analysed. In addition, using SBF, the Zn-coated samples were further analysed for its *in vitro* bioactivity.

2. Experimental procedure

2.1. Materials

Calcium nitrate ($Ca(NO_3)_2$; 99.9%; Merck AR), diammonium hydrogen phosphate ($(NH_4)_2HPO_4$; 99.9%; Merck AR), ammonium hydroxide (25%; Merck GR), and zinc nitrate (99.8%; Merck GR) were used as precursors. All the chemicals were used as such without any further purification. Ultrapure water (Arium 611 Ultrafilter; Sartorius AG, Germany) was used throughout the experiment.

2.2. HAp and ZnHAp nanocomposite preparation

HAp nanocomposites doped with different concentrations (0, 3 and 6 mol%) of zinc with a stoichiometric ratio of 1.67 were prepared through the ultrasonication process using a sonochemical reactor (VC 505; Sonics, USA). In this process, $Ca(NO_3)_2$ was dissolved in ultrapure water at room temperature under sonication at 30 kHz. After 15 min, zinc nitrate with different concentrations was added to the solution. To achieve the stoichiometric ratio, $(NH_4)_2HPO_4$ solution was added dropwise into $Ca(NO_3)_2$ solution. The pH of the solution was adjusted to 10.2 using ammonium hydroxide solution and the ultrasonication process was continued for 1 h. The HAp nanocomposites containing different mole percentages of zinc (i.e., 0, 3 and 6 mol%; hereafter termed HAp, Zn3HAp and Zn6HAp, respectively) were then filtered, washed and dried at 353 K for 12 h. Once dried, the precipitates of pure and zinc-doped HAp samples of all compositions were ground into a fine powder.

2.3. ZnHAp/CTS composite coating on the 316L SS substrate

Prepared HAp and ZnHAp powders (1 g) were individually mixed with 5% acetic acid solution containing 1 wt% CTS. The composites were ultrasonicated for 30 min at 30 kHz for uniform and complete dispersion. The dispersed polymer composites were coated on the 316L SS plate by spin coating technique. Before the coating, $10 \times 7\ mm^2$ SS specimens were mechanically polished using series silicon carbide papers (50–1600 grits). Then, the specimens were washed three times with acetone followed by distilled water. Two to three drops of the uniformly dispersed polymer composite solution containing ZnHAp were placed on the prepared 316L SS plate, which was then spin coated at 2500 rpm. The coated plate was then dried in a hot-air oven at 353 K. The coating and drying processes were repeated thrice for a better, thick and uniform coating. Finally, the coated plate was dried at 353 K for 12 h.

2.4. Characterisation

2.4.1. Size and composition measurement

The diameter of the HAp and ZnHAp samples was measured using dynamic light scattering (DLS; Nanophox; Sympatec, Germany) in the range of 1–500 nm with the scattering angle of 90°. The light source used was HeNe laser with a maximum intensity of 10 mW. Elemental composition of the prepared HAp and ZnHAp samples was determined using an X-ray fluorescence (XRF) spectrometer (EDX-720; Shimadzu, Japan). The Ca/P/Zn ratio in the HAp structure was measured.

2.4.2. Phase analysis

The phase purity and structural nature of the prepared HAp and ZnHAp samples were assessed using X-ray powder diffraction (XRD; X′Pert PRO; PANalytical, the Netherlands) with monochromatic Cu Kα as the radiation source (λ=1.540 Å). The scan was performed over a 2θ range of 20–80° with a scanning rate of 10°/min. To identify the position of the peak, the observed results were compared with the standard JCPDS file.

2.4.3. Functional group and morphological characterisation

The functional group characterisation of the prepared samples was verified using Fourier transform infrared spectroscopy (FTIR; Spectrum 100; PerkinElmer, USA) with the wave number range of 4000–400 cm^{-1} in the resolution of 1 cm^{-1}. The pellet for FTIR analysis was prepared by the KBr pellet method. The morphology of the coated plates was determined using scanning electron microscopy (SEM; model JSM 6390 LV; JEOL, Japan).

2.5. Electrochemical linear polarisation and impedance studies

Electrochemical polarisation and impedance spectroscopy studies of zinc-doped HAp samples were carried out using electrochemical workstation (PGSTAT302N; Metrohm Autolab, the Netherlands). A standard three-electrode cell assembly was used as a working cell with saturated calomel and a platinum electrode as a reference and a working electrode, respectively. The SBF with the ionic concentrations nearly equal to the human blood plasma was prepared using Kokubo method [19]. The prepared body fluid was used as the electrolyte for the corrosion study, the exposed area of the coated plates was 0.5 cm^2 and the remaining area was covered using an insulating tape. The electrochemical analysis was performed by immersing the electrodes in the electrolyte solutions. The corrosion current density, corrosion potential, rate of corrosion and impedance parameters were calculated on the basis of the polarisation graph.

2.6. Antimicrobial activity

Antimicrobial activity of the HAp and ZnHAp/CTS nanocomposites with microorganisms was measured using Kirby–Bauer disc diffusion method [20]. Various gram-positive (*Bacillus subtilis* and *Staphylococcus aureus*) and gram-negative (*Klebsiella pneumonia*, *Salmonella typhi* and *Pseudomonas aeruginosa*) microorganisms obtained from National Collection of Industrial Microorganisms (National Chemical Laboratory, Pune, India) were used to analyse the antimicrobial activity. The bacterial strains were subcultured and incubated at 310 K for 1 h. The antimicrobial tests were performed on the previously prepared, solidified and sterilised Mueller–Hinton agar plates. The discs were loaded with different concentrations of zinc-containing composites, that is, HAp/CTS, Zn3HAp/CTS and Zn6HAp/CTS, and incubated at 310 K for 24 h. After the incubation period, the inhibitory zone was measured and a graph was plotted. The bacteriological tests were performed in duplicate for better reproducibility of the results. The microbial resistance of the composites was measured from the inhibitory zone formed around the disc.

2.7. Bioactivity analysis

In vitro bioactivity of the HAp and ZnHAp/CTS composite-coated SS implant in physiological environment was determined by immersing the implant in SBF for 3 weeks incubation at 310 K in a water bath shaker. After incubation, the plates were washed using ultrapure water and dried at 373 K. The bone-like apatite layer formation on the surface of the coated implant was analysed using XRF and SEM analyses.

3. Results and discussions

3.1. Size and structure of ZnHAp nanocomposite

Fig. 1 shows the unimodal particle size distribution of pure and zinc-doped HAp samples. The size of individual nanoparticle is determined by the DLS method. The particle diameters of HAp, Zn3HAp and Zn6HAp are found to be 54.3, 34.6 and 17.2 nm, respectively. From the results, it is observed that as the concentration of zinc increases the plot shifts to smaller particle diameter, indicating the decrease in particle size with the distribution of average mean size. It is clear that the incorporation of zinc in HAp strongly influences the particle size. From this result, it is confirmed that the zinc ions are incorporated in the HAp structure. Fig. 2 presents the XRD pattern of the 0–6 mol% zinc-substituted HAp samples. The observed pattern shows pure apatite phase without any additional phase (calcium phosphate or zinc phosphate). The intense

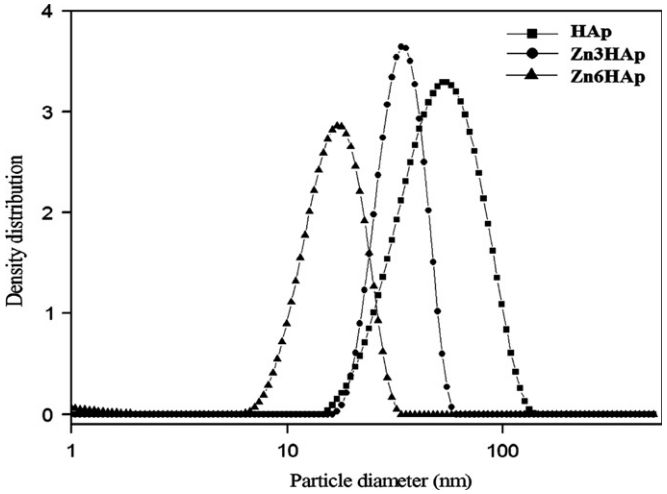

Fig. 1. Particle size distribution of HAp and Zn-doped HAp dispersed in water.

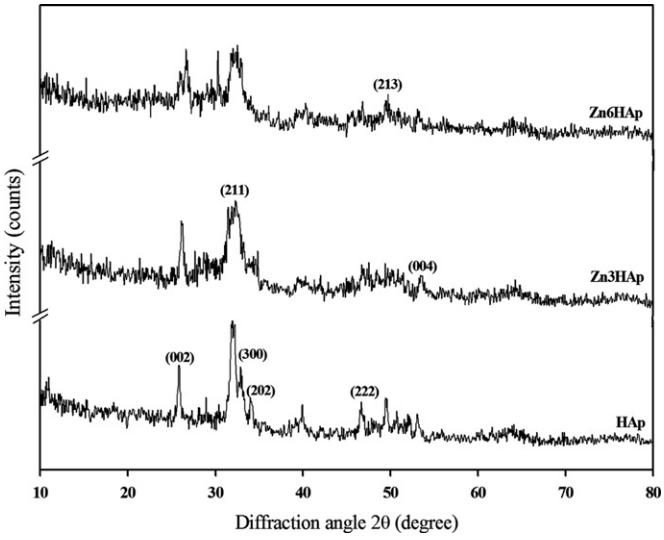

Fig. 2. X-ray diffraction pattern of the as-synthesised HAp and Zn-doped HAp nanoparticles.

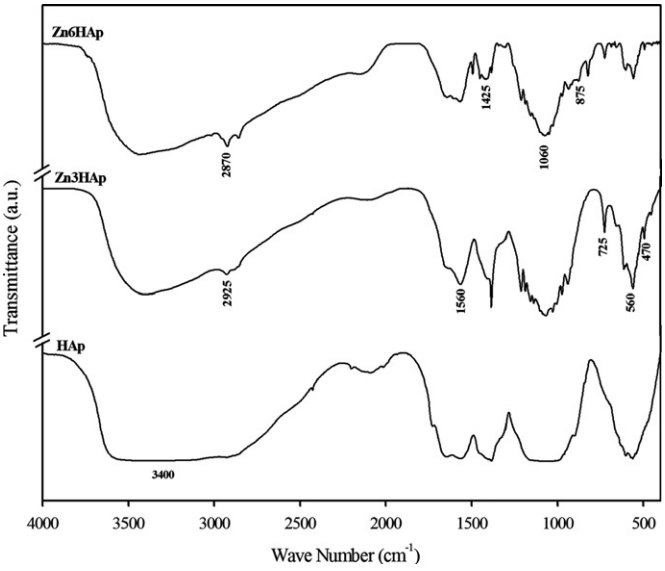

Fig. 3. Infrared spectra of the HAp and Zn-doped HAp nanoparticles.

diffraction peaks corresponding to HAp at the diffracted angles 25.71°, 31.95°, 32.88°, 34.1°, 39.99° and 46.69° indicate crystalline nature of the HAp synthesised using the ultrasonication process [21]. However, the introduction of zinc ion in the HAp structure clearly reduces the crystalline peak intensity with wider distribution. From this observation, it is clear that the incorporation of zinc in the HAp structure influences the degree of crystallinity. The increase in the concentration of zinc highly reduces the crystallinity of the HAp crystal, because higher concentration of zinc inhibits the apatite crystal growth by separating the grain boundaries.

The infrared spectrum in Fig. 3 shows the complex nature of the ZnHAp/CTS composite. All spectra show similar peaks corresponding to the HAp crystals and several common peaks due to the presence of CTS polymer in the composite. The intense broad absorption band observed in the range of 3000–3400 cm^{-1} corresponds to the stretching vibration of OH^- ions in the structure. The multiplets located around 1000 cm^{-1} are developed by phosphate modes. The absorption bands observed in the regions of 560 and 1060 cm^{-1} correspond to the stretching vibration of PO_4^{3-} ions [22]. The absorption peaks observed at 875 and 1425 cm^{-1} correspond to the air-absorbed CO_3^{2-} ions. The band observed at 602 cm^{-1} corresponds to O–P–O bending and symmetric P–O stretching vibrations [23]. The weak absorption bands observed at 2925 and 2846 cm^{-1} correspond to asymmetrical and symmetrical stretching vibrations of $C–CH_2$. The peak observed at 1580 cm^{-1} corresponds to the bending vibration of primary amine of CTS molecule [24]. Apart from the peaks absorbed for HAp and CTS, no additional peak is found in the spectrum, confirming the absence of interbonding between HAp and CTS.

3.2. Electrochemical evaluation of the coating

The surface resistivity and protective properties of the HAp with different concentrations of the ZnHAp/CTS composite-coated implant in SBF are evaluated through potentiodynamic polarisation studies. The results obtained are shown in Fig. 4. The polarisation curve for the ZnHAp/CTS composite-coated SS substrate is substantially different from that of the HAp/CTS composite-coated substrate. During electrochemical analysis, the SS plate coated with HAp and ZnHAp composites influences the corrosion properties. From the potentiodynamic polarisation analysis, it is observed that the ZnHAp/CTS composite-coated SS plate shows a high shift in the potential than that of the HAp/CTS composite coated implant. However, increase in zinc percentage in HAp composition increases the breakdown potential in the noble direction.

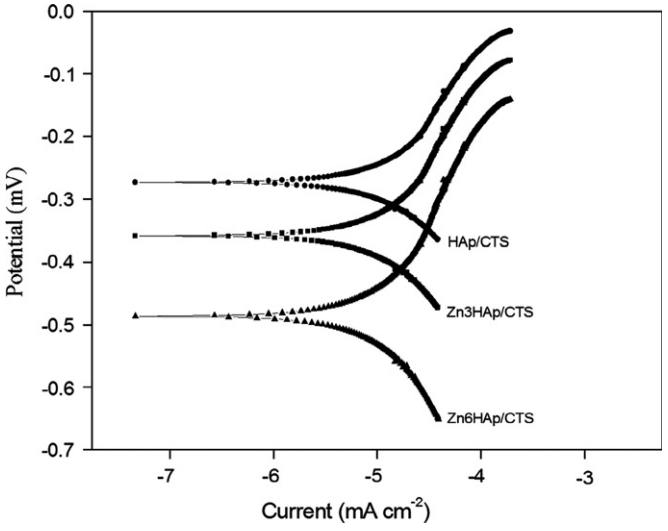

Fig. 4. Potentiodynamic polarisation curve of the HAp and Zn-doped HAp/CTS composite-coated 316L SS plate in SBF solution.

Table 1
Corrosion parameters of HAp and ZnHAp/CTS coated 316L SS implant in simulated body fluid.

Sample code	Corrosion current density ($i_{corr} \times 10^{-5}$)	Corrosion potential ($E_{corr} \times 10^{-3}$)	Polarisation resistance ($R_p \times 10^3\ \Omega\ cm^2$)	Rate of corrosion (mm/year $\times 10^{-2}$)
HAp/CTS	1.82	−516.52	1.6502	21.10
Zn3HAp/CTS	1.1	−512.15	1.9837	12.79
Zn6HAp/CTS	0.833	−422.47	2.0891	9.806

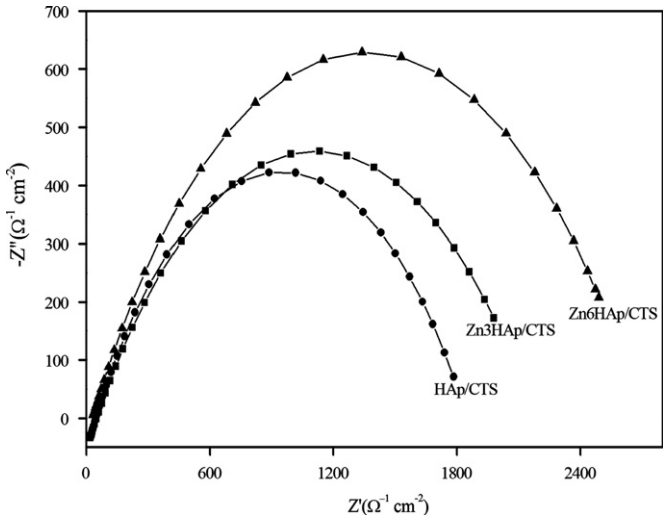

Fig. 5. Nyquist impedance curves for the HAp and Zn-doped HAp/CTS composite-coated 316L SS plate in SBF solution.

The corrosion current density (i_{corr}), corrosion potential (E_{corr}), polarisation resistance (R_p) and rate of corrosion (millimetre/year) obtained from the polarisation curve are shown in Table 1. The ZnHAp/CTS composite coating reduces the corrosion current density (i_{corr}) more than the HAp/CTS composite-coated substrate and acts as an efficacious passive layer that effectively reduces the active surface area. The breakdown potential of the ZnHAp/CTS coating was more than that of the HAp/CTS coatings. The observed results indicate that the composite having zinc ions in its structure acts as a protective layer, inhibiting the corrosion rate of the coated implant. The extracted graph shows that the corrosion current density (i_{corr}) of the HAp/CTS composite-coated 316L SS plate was 1.8×10^{-5}, whereas that for the 3 and 6 mol% ZnHAp/CTS composite-coated 316L SS plates was 1.1×10^{-5} and 8.33×10^{-6}, respectively. The corrosion current density (i_{corr}) decreases with increase in the percentage of zinc in HAp layer composition, leading to an increase in corrosion resistance of the ZnHAp composite-coated implant.

Fig. 5 shows the impedance graph of the HAp and ZnHAp/CTS composite-coated 316L SS implant in the SBF. Generally, Nyquist plots show a semicircle for all the coatings, the diameter of which increases with respect to the increase in the polarisation resistance, as shown in Fig. 5. The polarisation resistance (R_p) values of the coated implant extracted from the graph are shown in Table 1. It is clear that the polarisation resistance of the 6 mol% ZnHAp/CTS composite-coated 316L SS implant is more than that of the HAp/CTS composite-coated implant. The higher R_p values show higher corrosion resistance, which is increased nearly 2.6584×10^4 with respect to the concentration of zinc. The ZnHAp composite coating acts as a barrier against attack of anions, effectively improve the corrosion resistance of the 316L SS implant. The samples coated with higher zinc percentage show that zinc can act as a protective layer against corrosion in the physiological environment. The increase in corrosion resistance with the increase in zinc concentration may be due to the uniform coating of passive layer on the surface of the 316L SS plate. These results show that the ZnHAp/CTS composite is a better alternative anticorrosion coating for implant applications.

3.3. Antimicrobial activity

Antimicrobial activity of the HAp and ZnHAp/CTS composites against the gram-positive and gram-negative bacterial strains such as *B. subtilis*, *S. aureus*, *K. pneumonia*, *S. typhi* and *P. aeruginosa* is investigated using the disc diffusion method. The inhibitory zone of the bacterial strain with respect to the zinc concentration in HAp is analysed. The nanocomposites show significant amount of antimicrobial activity, as shown in Fig. 6. The HAp shows maximum antimicrobial activity of 0.9 mm diameter zone against gram-positive bacterial strains than against the gram-negative ones. However, it is clear that the incorporation of zinc ions in the HAp lattice improves its antimicrobial properties. The maximum concentration of zinc shows maximum inhibition zone of 15 mm against the gram-negative bacterial strains *Klebsilla* sp. and *Pseudomonas* sp. Thus, the increase in antimicrobial activity against the bacterial strains may be due to the interaction between the nanocomposites and the bacterial cell membrane via the electrostatic attraction. This attraction leads to bacterial adhesion on the apatite surfaces. Similarly, the increase in bacterial adhesion with increasing zinc concentration leads to the inhibition of bacterial growth.

3.4. In vitro analysis of the coating

Microstructure and morphology of the coating before and after immersion in SBF for 21 days are examined using SEM. Fig. 7(a–c) presents the SEM morphologies of

the HAp, Zn3HAp/CTS and Zn6HAp/CTS composite-coated implants obtained by spin coating technique. It can be seen from Fig. 7(a) that the HAp/CTS coating leads to the changes on the surface, whereas introduction of zinc ion into the HAp lattice improves uniformity of the coating, without any cracks or microspores. There are obvious differences between the undoped and zinc-doped HAp coatings. When the zinc concentration reaches 6 mol%, the area of the coated plate is almost absolutely covered by the ZnHAp/CTS composite and uniform coating is achieved because of the small particle diameter of Zn6HAp. To evaluate the formation of bone-like apatite layer, we performed SEM investigation on the surface of the implant after immersion in SBF for 21 days, as shown in Fig. 8(a–c). From the figure, it is observed that the microstructure of the implant immersed in SBF is totally different from that of the coated implant before and after immersion in SBF. The image obtained after 21 days indicates newly formed apatite on the surface of the implant in the form of white agglomerates. The formation of apatite layer increases with increase in zinc concentration in the HAp structure. The maximum apatite layer formation is observed for the HAp-coated implant with 6 mol% of zinc.

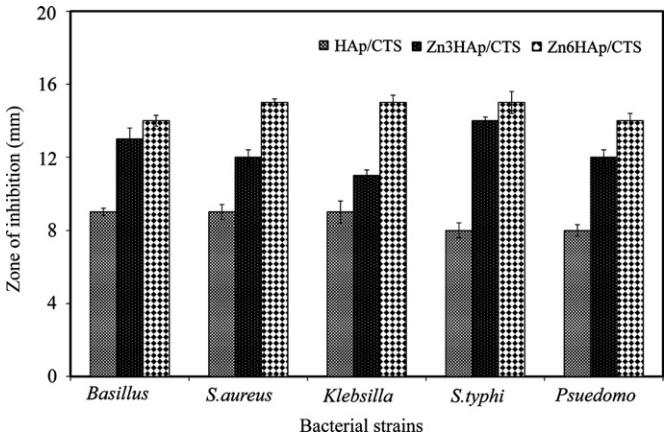

Fig. 6. Antimicrobial activity of the HAp and Zn-doped HAp/CTS composites with various gram-positive and gram-negative bacterial strains.

The formation of apatite layer on the surface of the ZnHAp/CTS composite is further confirmed by XRF analysis. The XRF results indicate that the obtained 0, 3 and 6 mol% ZnHAp nanoparticles are in the stoichiometric ratio of 1.68, 1.63 and 1.65, respectively. Further, it is observed that the plates immersed in SBF the content and ratio of the Ca and P ions increased in the surface of the implant to 1.72, 1.69 and 1.73. However, a slight decrease in Zn content is also observed for the 316L SS implant coated with ZnHAp/CTS containing 3 and 6 mol% of zinc. The decrease in Zn concentration during the *in vitro* analysis may be due to dissolution of the ZnHAp sample in coating and also because of the thick apatite layer formation above the coated implant. Thus, it is confirmed that the ZnHAp/CTS composite improves the formation of bioactive HAp layer on the surface of the coated implant. However, the Zn6HAp/CTS coated sample shows higher HAp formation. From all the above studies, it is concluded that the Zn-doped HAp/CTS composites show excellent bioactivity with enhanced

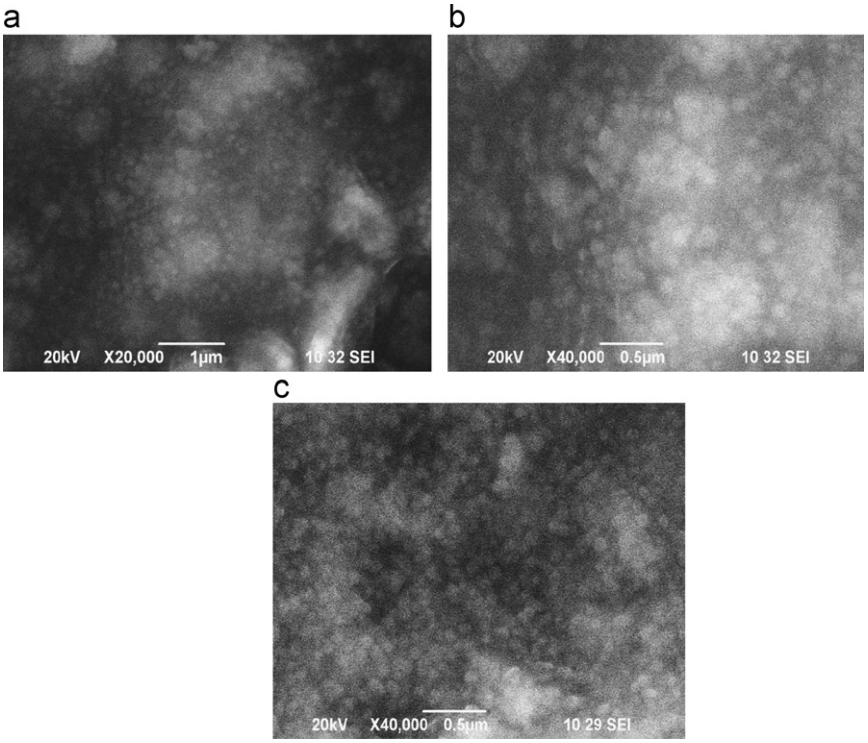

Fig. 7. SEM image of the 316L SS implant surface coated with (a) HAp/CTS, (b) Zn3HAp/CTS and (c) Zn6HAp/CTS composites.

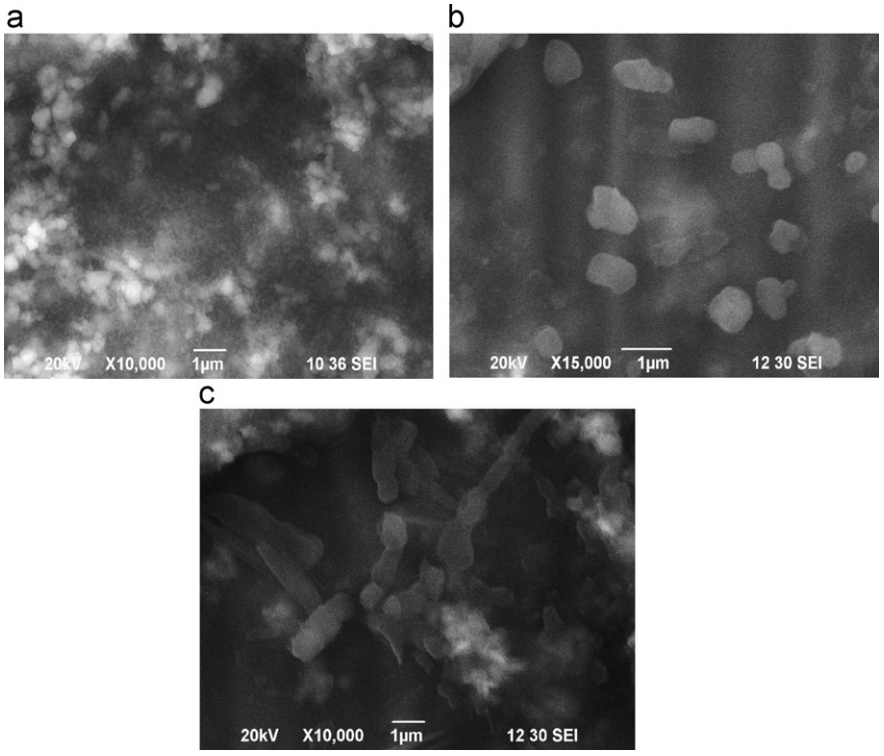

Fig. 8. SEM images of the 316L SS plate coated with (a) HAp/CTS, (b) Zn3HAp/CTS, and (c) Zn6HAp/CTS composites after immersion in SBF for 21 days.

antimicrobial activity and corrosion resistance. The implant coated with Zn-doped HAp/CTS is a better alternate in biomedical implant applications because of effective antimicrobial properties.

4. Conclusion

HAp and ZnHAp powders with nanometer range were obtained through the ultrasonication process. The HAp and ZnHAp/CTS composite coating on the SS plate was carried out using spin coating technique. Their elemental composition analysed by XRF shows the stoichiometric ratio of the prepared HAp. Functional group analysis from FTIR confirms the presence of the HAp/CTS composite. The electrochemical polarisation and impedance spectroscopy analyses of the HAp and ZnHAp/CTS composite-coated implant were carried out in SBF. These analyses confirm the significant increase in the surface properties of the 316L SS plate. An increase in the zinc concentration in the HAp structure significantly increases the resistivity of the SS implant. The observed results indicate that the coating of HAp with 6 mol% of zinc has the highest corrosion resistivity in the physiological solution. In addition, the enhanced antimicrobial property of HAp was observed with the high zinc concentration. The increased formation of apatite layer on the surface of the implant is observed for Zn6HAp/CTS. Thus, it is clear that ZnHAp/CTS will be a better material for active coating for lifetime implant application.

References

[1] D. Gopi, V. Collins Arun Prakash, L. Kavitha, S. Kannan, P.R. Bhalaji, E. Shinyjoy, J.M.F. Ferreira, A facile electrodeposition of hydroxyapatite onto borate passivated surgical grade stainless steel, Corrosion Science 53 (2011) 2328–2334.

[2] S. Kannan, A. Balamurugan, S. Rajeswari, H_2SO_4 as a passivating medium on the localised corrosion resistance of surgical grade 316L SS metallic implant and its effect on hydroxyapatite coatings, Electrochimica Acta 49 (2004) 2395–2403.

[3] Z. Bou-Saleh, A. Shahryari, S. Omanovic, Enhancement of corrosion resistance of a biomedical grade 316LVM stainless steel by potentiodynamic cyclic polarisation, Thin Solid Films 515 (2007) 4727–4737.

[4] V. Muthukumaran, V. Selladurai, S. Nandhakumar, M. Senthilkumar, Experimental investigation on corrosion and hardness of ion implanted AISI 316L stainless steel, Materials & Design 31 (2010) 2813–2817.

[5] C.T. Kwok, P.K. Wong, F.T. Cheng, H.C. Man, Characterization and corrosion behaviour of hydroxyapatite coating on Ti6Al4V fabricated by electrophoretic deposition, Applied Surface Science 255 (2009) 6736–6744.

[6] C. Wen, S. Guan, L. Peng, C. Ren, X. Wang, Z. Hu, Characterisation and degradation behaviour of AZ31 alloy surface modified by bone-like hydroxyapatite for implant applications, Applied Surface Science 255 (2009) 6433–6438.

[7] Y. Chen, X. Miao, Effect of fluorine addition on the corrosion resistance of hydroxyapatite ceramics, Ceramics International 30 (2004) 1961–1965.

[8] K. Matsunaga, H. Murata, T. Mizoguchi, A. Nakahira, Mechanism of incorporation of zinc into hydroxyapatite, Acta Biomaterialia 6 (6) (2010) 2289–2293.

[9] K. Cheng, J. Zhou, W. Weng, S. Zhang, G. Shen, P. Du, G. Han, Composite calcium phosphate coatings with sustained Zn release, Thin Solid Films 519 (15) (2011) 4647–4651.

[10] R.J. Cheng, M.F. Hsieh, K.C. Huang, L.H. Perng, F.I. Chou, T.S. Chin, Anti-microbial hydroxyapatite particles synthesised by a

sol–gel route, Journal of Sol–Gel Science and Technology 33 (2005) 229–239.
[11] F. Ren, R. Xin, X. Ge, Y. Leng, Characterization and structural analysis of zinc substituted hydroxyapatites, Acta Biomaterialia 5 (2005) 3141–3149.
[12] A. Ito, H. Kawamura, M. Otsuko, M. Ikeuchi, H. Ohgushi, K. Ishikawa, K. Onuma, N. Kanzaki, Y. Sogo, N. Ichinose, Zinc-releasing calcium phosphate for stimulating bone formation, Materials Science and Engineering C: Materials for Biological Applications 22 (2002) 21–25.
[13] Y. Tang, H.F. Chappell, M.T. Dove, R.J. Reeder, Y.J. Lee, Zinc incorporation into hydroxylapatite, Biomaterials 30 (2009) 2864–2872.
[14] W. Xue, K. Dahlquist, A. Banerjee, A. Bandyopadhyay, S. Bose, Synthesis and characterization of tricalcium phosphate with Zn and Mg based dopants, Journal of Materials Science: Materials in Medicine 19 (2009) 2669–2677.
[15] X. Pang, I. Zhitomirsky, Electrodeposition of composite hydroxyapatite–chitosan films, Materials Chemistry and Physics 94 (2005) 245–251.
[16] X. Pang, I. Zhitomirsky, Electrophoretic deposition of composite hydroxyapatite–chitosan coatings, Materials Characterization 58 (2007) 339–348.
[17] Q. Hu, B. Li, M. Wang, J. Shen, Preparation and characterization of biodegradable chitosan/hydroxyapatite nanocomposite rods via in situ hybridization: a potential material as internal fixation of bone fracture, Biomaterials 25 (2004) 779–785.
[18] J. Zhang, G. Liu, Q. Wu, J. Zuo, Y. Qin, J. Wang, Novel mesoporous hydroxyapatite/chitosan composite for bone repair, Journal of Bionic Engineering 9 (2012) 243–251.
[19] A. Oyane, H.M. Kim, T. Furuya, T. Kokubo, T. Miyazaki, T. Nakamura, Preparation and assessment of revised simulated body fluids, Journal of Biomedical Materials Research A 65 (2003) 188–195.
[20] A.W. Bauer, W.M. Kirby, J.C. Sherris, M. Turch, Antibiotic susceptibility testing by a standardized single disk method, American Journal of Clinical Pathology 45 (1966) 493–496.
[21] R.M.B. Faria, D.V. Cesar, V.M.M. Salim, Surface reactivity of zinc-modified hydroxyapatite, Catalysis Today 133 (2008) 168–173.
[22] Y. Li, D. Li, W. Weng, Preparation of nano carbonate-substituted hydroxyapatite from an amorphous precursor, International Journal of Applied Ceramic Technology 5 (2008) 442–448.
[23] M.J. Ma, Y.J. Zhu, J. Chang, Monetite formed in mixed solvents of water and ethylene glycol and its transformation to hydroxyapatite, Journal of Physical Chemistry B 110 (2006) 14226–14230.
[24] C. Xu, D. He, L. Zeng, S. Luo, A study of adsorption behavior of human serum albumin and ovalbumin on hydroxyapatite/chitosan composite, Colloids and Surfaces B: Biointerfaces 73 (2009) 360–364.